P4.3

THE FOG REMOTE SENSING AND MODELING (FRAM) FIELD PROJECT AND PRELIMINARY RESULTS

I.Gultepe[1,2], S.G. Cober[1], G. A.Isaac[1], [1]D. Hudak, P. King[1], [3]P. Taylor, [3]M. Gordon, [1]P. Rodriguez, B. Hansen[1], and M. Jacob[1]

[1]Cloud Physics and Severe Weather Research Section, Science and Technology Branch, Environment Canada Toronto, Ontario, M3H 5T4, Canada

[3]Centre for Research in Earth and Space Science, York University, Toronto, Ontario. M3J 1P3 Canada

1. INTRODUCTION

The purpose of the Fog Remote Sensing And Modeling (FRAM) field project is to characterize fog formation, evolution, and dissipation in continental and marine environments, and then to use the derived results in numerical model simulations and remote sensing applications. Phase 1 of the project took place over the Center for Atmospheric Research Experiment (CARE) site (FRAM-C) during the winter of 2005-2006 in southern Ontario. Phase 2 of the project took place over Lunenburg site (FRAM-L) in Nova Scotia near the Atlantic coast during the summer of 2006. These two phases focus on winter continental fog and summer marine fog, respectively.

Fog forecasting/nowcasting cannot be successful until a better understanding of fog microphysics and the large/small scale effects on its formation is provided. The current parameterization for fog visibility (vis) in numerical models is not accurate (Stoelinga and Warner, 1999; Gultepe et al., 2006). Ellrod (1995) stated that satellite observations can help for fog forecasting at night time because of the SW contribution from clouds during the day time. An integration of surface based sensors, remote sensors and model data, as proposed by Isaac et al. (2006) for airport winter weather, might help provide improved predictions/nowcasts.

During the winter of 2005-2006, an increased frequency of fog formation was observed in southern Ontario relative to the 30-year climatology. It is suggested that events with a combination of snow on the surface with rain falling from above caused this increase in frequency. Rain falling on a snow surface resulted in a release of latent heat which caused evaporation of snow, higher boundary layer saturations, and fog formation. Overall, a summary of observations together with some microphysical parameterizations are provided.

2. OBSERVATIONS

Observations were collected during FRAM-C from Dec. 1, 2005 to April 18, 2006. The total number of cases with vis<1 km was 15. Here, we present results for the January 4 and April 15 cases that represent warm fog, and for the March 10 case that represents freezing/ice fog. Observations collected during the winter of 2005-06 include droplet, ice, aerosols sizes and concentrations from optical probes, visibility from a Vaisala visibility meter, liquid water content (LWC), relative humidity with respect to water (RHw), temperature (T), liquid water path (LWP) from a microwave radiometer (MWR), and inferred fog properties such as drop diameter, liquid water content, and number concentration, and fog regions from satellites.

Table 1: The list of instruments for FRAM projects.

Instrument	FRAM-C	FRAM-L	Measurement	Measurement range or comment
DMT FMD SPP-FM	x	x	Droplet size, LWC, and N_d	0-50 micron
FSSP	x	-	Droplet size, LWC, N_d	0-48 micron
PCASP	x	-	Aerosol size, mass, and concentration	0.1-3 micron
Hot Plate	x	-	precipitation rate	-
York University ice particle counters (IPC)	x	-	Number concentration and particle flux	10-500 micron
MWR1100	x	-	LWP,T, vapor mixing ratio (qv)	>0.05 g m^{-2}
MWR TP3000	x	x	LWC, T, qv	>0.05 g m^{-2}
Vaisala FD12P	x	x	Visibility, precipitation type, intensity	-
Vaisala Ceilometer CT25K	x	x	Cloud base height and backscatter profile	-
POSS	x	-	precipitation type and intensity	-
Climatronic aerosol profiler	-	x	Aerosol size and concentration	0.3-10 micron 8 channels
Clearvue video unit	-	x	Images and visibility	-
Young 81000 Sonic anemometer	-	x	3D wind speed and turbulence	4-32 Hz sampling rate
Eppley IR and SW Radiometers	x	x	Broadband radiative fluxes	-
Buoys	-	x	Temperature, RH, and wind	1Hz sampling rate
Wind profiler	x	x	Temperature, wind	Output at 1 min averages
Campbell Scientific HMP45C	x	x	Temperature and RH	-

[2]*Corresponding author: Dr. Ismail Gultepe, Cloud Physics and Severe Weather Research Section, Science and Technology Branch, Environment Canada, Toronto, Ontario, M3H 5T4, Canada. Email:ismail.gultepe@ec.gc.ca*

The pictures of some instruments shown in Fig. 1 are the Droplet Measurement Systems (DMT) fog measuring device (FMD), Vaisala ceilometer CT25K, York University ice particle counters (IPC, Savelyev et al., 2003; Brown and Pomeroy, 1989) mounted on a 10 m tower, DRI Hot Plate, PMS forward scattering spectrometer probe (FSSP), PMS particle cavity axial spectrometer probe (PCASP), and FMD combination, Radiometrics MWR radiometers (profiling and regular ones), Vaisala FD12P, and the Precipitation Occurrence Sensor System (POSS). Table 1 summarizes the instrument list from FRAM-C and FRAM-L but the results from only FRAM-C will be given here.

3. ANALYSIS AND RESULTS

The visibility (vis) calculations from the FMD probe is obtained using the following formula where the extinction coefficient is obtained using a well know Mie theory for droplets:

$$\beta_{ext} = \sum Q_{ext} n(r) \pi r^2 dr \qquad (1)$$

where *n* is the number density of particles in a bin size as radius *(r)* and Q_{ext} is the Mie extinction coefficient. Q_{ext} is related to number concentration, particle radius, and the wavelength of visible light. When the drop size increases larger than about 4 μm, Q_{ext} becomes 2. It fluctuates between 3.8 and 0.9 for particle sizes less than 4 μm. (Koenig, 1971). The extinction parameter is converted to v*is* using an equation given by (Stoelinga and Warner, 1999) as

$$vis = -\ln(0.02) / \beta_{ext}\,. \qquad (2)$$

For ice fog, vis measurements are obtained from the Vaisala FD12P data and plotted against IPC measurements where wind speed was significantly smaller than blowing snow conditions (>4 m s^{-1}). The following equations are used for calculations of the IPC ice particle number flux and ice fog number concentrations:

$$N_{if} = C / A\,, \qquad (3)$$

and

$$N_i = C / AU_w\,, \qquad (4)$$

where C is the average number of particles per second crossing their beams (Hz), A is the beam cross section area (m^2), N_{if} and N_i are the ice particle number flux (m^{-2} s^{-1}) and ice crystal number concentration (L^{-1}), respectively. Uw is the horizontal wind speed measured at the 10 m tower. The A values for IPC1 (at 0.7 m) and IPC2 (at 2.5 m) were 6.15e-6 m^2 and 5.85e-6 m^2, respectively. In the N_i calculations, we assumed that Uw at 10 m was also representative of the winds at about 2 m because ice fog conditions occurred at calm wind conditions (<3 m s^{-1}).

a) Climatology of FRAM project areas from 1970 to 2004

The FRAM field project took place in the two regions as described above. The climatology of both Toronto Pearson International Airport in Ontario and Halifax International airport in Nova Scotia are shown in Figs. 2a and 2b, respectively. Fig 2a shows that high frequency of fog formation (up to 5%) at Pearson Airport with vis less than 0.5 miles, occurred during the October and March time periods in which the FRAM-L project took place. The fog frequency reached up to 30% of the time during May-August for the Halifax Airport (Fig. 2b). Based on these observations, FRAM-L took place in the Halifax area in June 2006.

b) Results from FRAM project

Measurements collected during FRAM-C were used in the analysis and some relationships between vis and fog microphysical parameters were derived. Figs. 3a and 3b show the warm and cold fog conditions that occurred on January 4 and March 9, respectively. A picture for the April 15 case was not available. It is seen that, for the January 4 case, snow was at the surface and some precipitation as rain occurred before the fog event.

1) January 4 case

For January 4, The RUC model based T and dew point temperature (Td) profiles (Fig. 4a) show that the boundary layer was saturated up to 800 mb and the wind speed was about 5 m s^{-1}. The GOES ch2 image (Fig. 4b) shows that some patchy low clouds/fog were present just north-west of Toronto. Visibility obtained from the Vaisala vis meter was about less than 0.5 km (Fig. 4c) at about 20:00-22:00 UTC. The time-height cross section of LWC and RHw from the MWR TP3000 shows that an elevated layer of stratiform cloud was just above the 1 km height and below it RH~100%. T at the surface was about 5°C. At the same time, LWC=0.05 to 0.1 g m^{-3} was observed over the surface (Fig. 4d). Fig. 4e shows that RHw was about 100% from the surface up to 3.5 km, indicating that some mid-level clouds were present.

Time series of the 1-s N_d data from the FMD indicated that max N_d reached up to 100 cm^{-3} (Fig. 5a) and vis corresponding to that value was about 500 m (Fig. 5b). It is clearly seen that increasing N_d resulted in lower vis values. Bimodal size distributions are seen in the FMD droplet spectra (Fig. 5c). A separation at about 15 micron size was likely due to the presence of drizzle size droplets with sizes > 15 micron.

The FMD measurements were used to obtain relationships between vis and N_d, LWC, and their combinations. During the analysis, it was found that LWC increases with increasing N_d (not shown) and the vis decreases with increasing N_d (Fig. 5d). Based on these observations, the following relationships using 1 minute averages were derived for vis parameterization for the January 4 case as

$$vis = 1.13 \left(LWCxN_d \right)^{-0.51}\,, \qquad (5)$$

and the fog settling rate as

$$V_t LWC = 73138 \left[\; LWC^{5/3} N_d^{\;(-2/3)} \;\right]^{1.10} \qquad (6)$$

where the units are [km] and [g m^{-2} h^{-1}] for Eq. 1 and 2, respectively. V_t is the concentration weighted particle terminal velocity. These fits are obtained from the bin averaged values of related parameters as shown in Figs. 5e and 5f.

2) April 15 case

For the April 15 case, T was about 14°C and warm fog occurred after a precipitation event, but snow was not present at the surface as in the January 4 case. Fig. 6a shows the results from the BUFKIT software that was based on a forecast model. It showed that vis was less than 0.5 miles (04:00 UTC), wind speed was approximately 3 m s^{-1} from south, and T~15°C (RH~100%). Precipitation during the fog event was not present, but a 10 mm/h precipitation rate (PR) was recorded at 3:25 UTC (not shown) before the fog occurred. Fig. 6b shows the fog regions at 02:00 UTC calculated based on the GOES algorithm as described by Gultepe et al. (2006). In this plot, the foggy area was likely under high level clouds. Fig. 6c shows the time series of vis which was less than 0.5 km for almost a 6 hour time period. The MWR TP3000 LWC profile (Fig. 6d) at about 4:00 UTC indicated that LWC was about 0.5 g m^{-3}. This high value of LWC was likely overestimated in this case because of wetting conditions on the radiometer window. The FMD measurements were found much smaller than MWR LWC, further verifying that wetting was an important issue. Fig. 6e shows the RHw time-height cross-section in which RHw is about 100%, matching with the fog occurrence. This figure also indicates that the vertical profile of RHw was not consistent with LWC.

Time series of the 1-s N_d and vis data from FMD are shown in Figs. 7a and 7b, respectively. The maximum N_d reached up to 250 cm^{-3} where vis was 250 m for about 0.5 hours. It is clearly seen that increasing N_d resulted in lower vis values. The bimodal size distributions are not seen in the FMD droplet spectra as indicated for the January 4 case (Fig. 7c) but the droplet concentration for sizes less than 5 micron was almost two times more than for the January 4 case.

Similar to the January 4 case, observations such as in Fig. 7d are used to obtain the relationships between vis and other microphysical parameters. Using 1 minute averages, vis parameterization on April 15, representing lower visibility conditions, is obtained as

$$vis = 1.02\left(LWCxN_d\right)^{-0.52}, \qquad (7)$$

and the fog settling rate as

$$V_t LWC = 58086\left[\ LWC^{5/3} N_d^{\ (-2/3)}\ \right]^{1.12} \qquad (8)$$

where the units are [km] and [g m^{-2} h^{-1}] for Eq. 1 and 2, respectively. These fits are shown over 1 min data points in Figs. 7e and 7f, respectively. Note that Eqs. 5 and 7 are very similar while Egs. 6 and 8 show some differences.

3) Ice fog case (Feb. 10)

The observations for the Feb 10 case are shown in Fig. 8. Fig. 8a shows the time series of wind speed (Uw), indicating that usually it was less than 3 m s^{-1}. A max N_{if} (ice particle flux) of 0.08e06 m^{-2} s^{-1} (Fig. 8b) corresponds to a low visibility value between 700 and 1200 min (Fig. 8c). Using the corresponding Vaisala measurements, the vis values are plotted against N_i (obtained from Eq. 4) as shown in Fig. 8d. The eye-fitted line over the data shows that N_i increases gradually from 0.8 l^{-1} up to 50 l^{-1}. The vis values are between 1-2 km up to 50 km depending on N_i.

4. DISCUSSION AND CONCLUSIONS

In this work, preliminary results from the FRAM field program are summarized. Previous studies tried to correlate vis to LWC which is currently used in modeling studies. The present work indicated that vis should be parameterized as a function of both LWC and N_d. Gultepe et al. (2006) stated that if N_d is not included in forecasting models, vis values can include uncertainties more than 50%.

The settling rate of fog droplets is important for sustaining the fog presence within the boundary layer. Unless this settling rate is parameterized based on observations, the fog water content cannot be obtained directly using the model microphysics because of preset auto-conversion coefficients in the models. The derived relationships can easily be used with bulk microphysical parameterization when N_d is obtained from model thermodynamical variables such as T and/or moisture.

The droplet spectra showed a bimodal distribution for the first case but not for the second case. The vis was almost 2 times less when large drops forming the bimodal spectra were not present, indicating that preset particle spectral shape for fog modeling should be carefully chosen.

Ice fog microphysical characteristics are still not known in detail because of measurement difficulties at low fall velocities/wind speeds, and at colder temperatures. The results from this work showed that N_i is directly related to vis. Increasing N_i results in lower vis values which are found to be comparable to warm fog values. This problem of ice fog characterization needs to be more fully addressed.

Nowcasting for fog conditions needs an integration of observations and models data (e.g. Isaac et al., 2006). This work showed that MWR, FMD, Vaisala vis meter, POSS observations, and satellite based algorithms are needed for a better nowcasting algorithm. Gultepe (2006) showed that integration of model based parameters such as RHw and T at the surface together with satellite based algorithms can improve fog forecasting up to 30%.

Overall, additional observations from the FRAM-L will let us describe various marine fog conditions and their microphysics for numerical modeling and satellite based applications.

5. ACKNOWLEDGEMENTS

Funding for this work was provided by the Canadian National Search and Rescue Secretariat and Environment Canada. Some additional funding was also provided by the European COST-722 fog initiative project office. Technical support for the data collection was provided by the Cloud Physics and Severe Weather Research Section of the Science and Technology Branch, Environment Canada, Toronto, Ontario. Authors were also thankful to M. Wasey and R. Reed of Environment Canada for technical support during the FRAM.

6. REFERENCES

Brown, T. and Pomeroy J.W., 1989: A blowing snow particle detector. *J. Cold Regions Science and Technology*, **16**, 167-174.

Ellrod, G. P., 1995: Advances in the detection and analysis of fog at night using GOES multi-spectral infrared imagery. *Weather and Forecasting*, 10, 606-619.

Gultepe, I., M. D. Müller, and Z. Boybeyi' 2006: A New Visibility Parameterization for Warm Fog Applications in Numerical Weather Prediction Models, J. Appl. Meteor., in press.

Gultepe, I., 2006: Development of a satellite based fog detection scheme using model screen temperature. Paper in Short range forecasting methods of fog, visibility, and low clouds Workshop, Langen, Germany, 20 October 2005, In press.

Isaac, G.A., M. Bailey, S.G. Cober, N. Donaldson, N. Driedger, A. Glazer, I. Gultepe, D. Hudak, A. Korolev, J. Reid, P. Rodriguez, J. W. Strapp and F. Fabry, 2006: Airport Vicinity Icing and Snow Advisor. *AIAA 44th Aerospace Sci. Meeting and Exhibit*, Reno Nevada, 9-12 January 2006, AIAA-2006-1219.

Koening, L. R., 1971: Numerical experiments pertaining to warm-fog clearing. *Mon. Wea. Rev.*, 9, 227-241.

Pagowski, M., I. Gultepe, and P. King, 2004: Analysis and Modeling of an Extremely Dense Fog Event in Southern Ontario, *J. of Appl. Meteor.* 43, 3–16.

Savelyev, S.A., M. Gordon, J. Hanesiak, T. Papakourioki, and P.A. Taylor, 2003: Blowing Snow Studies in CASES Canadian Arctic Shelf Exchange Study (CASES). *Hydrological Processes*, 4, 817-827.

Stoelinga, M. T., and T. T. Warner, 1999: Nonhydrostatic, Mesobeta-scale model simulations of cloud ceiling and visibility for an east coast winter precipitation event. *J. Appl. Meteor*., 38, 385-404.

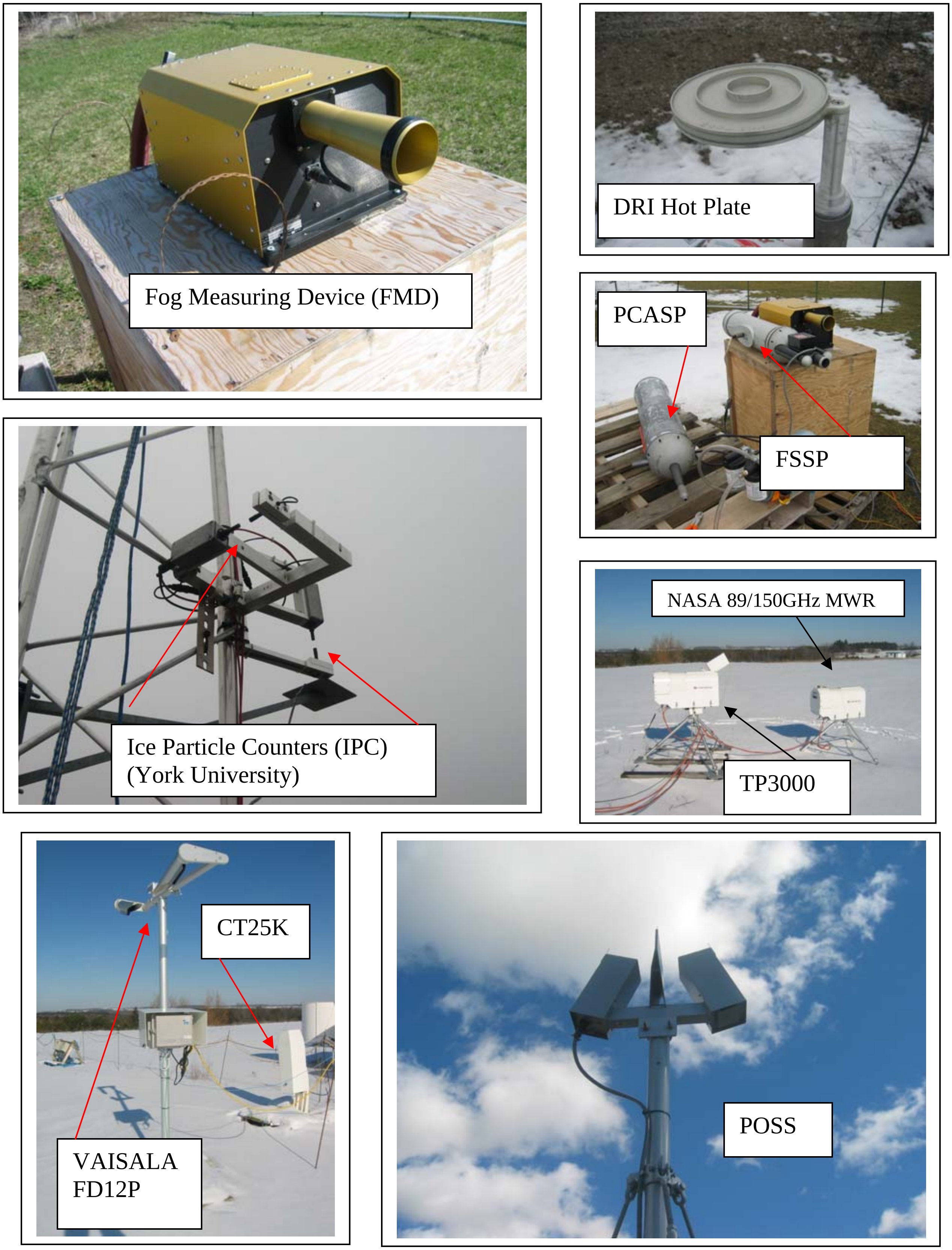

Fig. 1: Instruments used during FRAM-C.

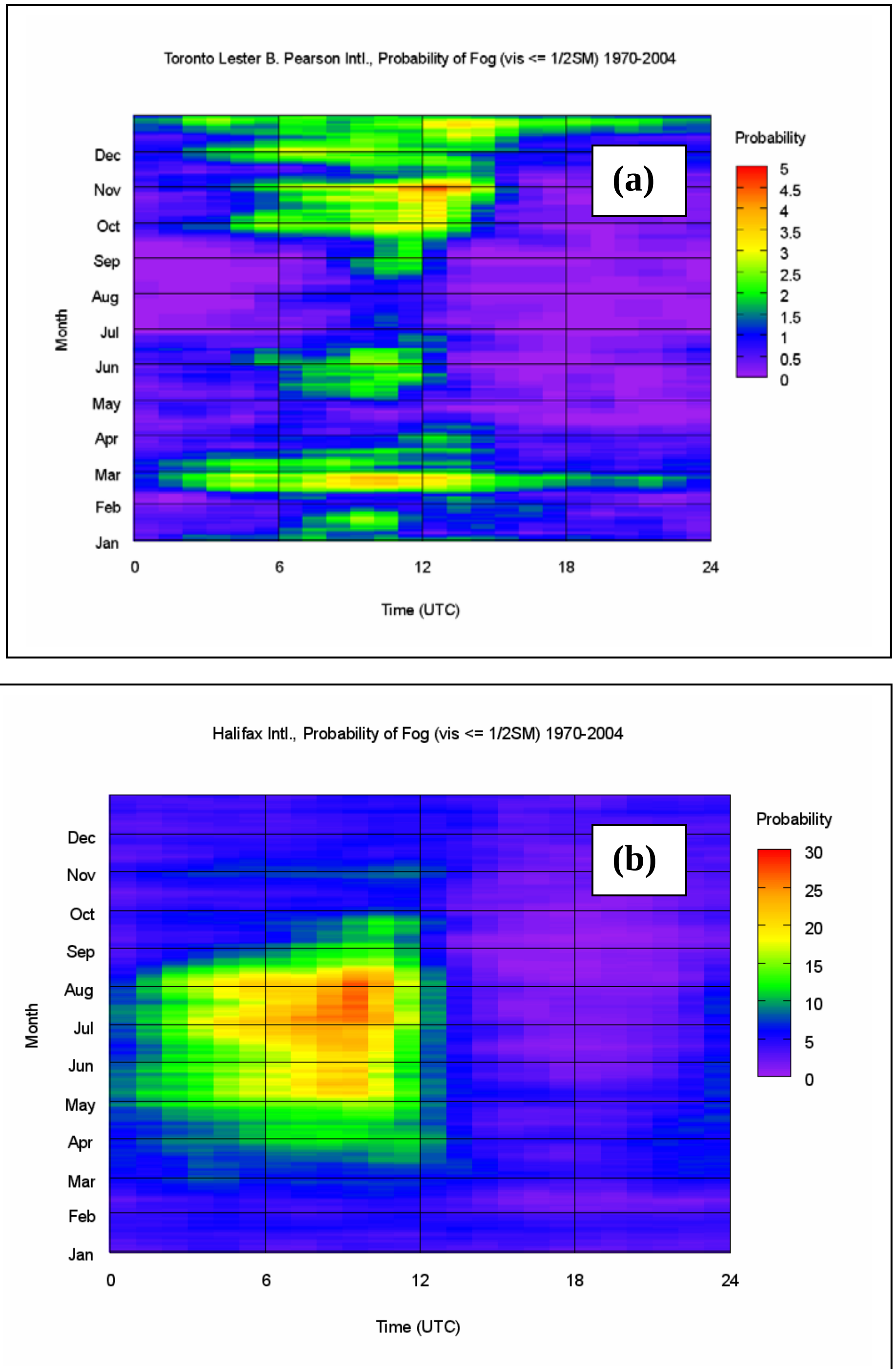

Fig. 2: Fog climatology of Toronto Pearson Airport and Halifax International airport.

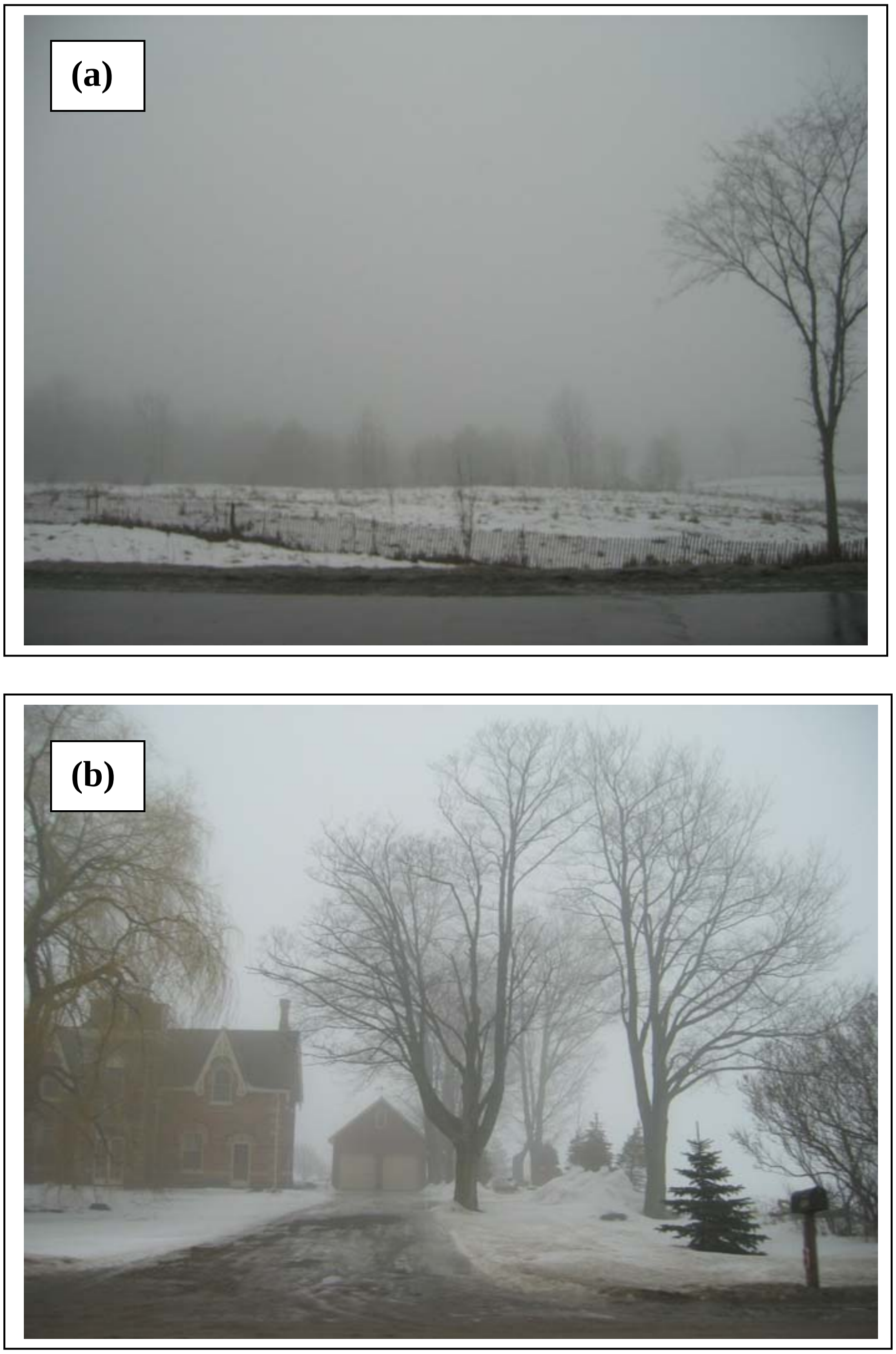

Fig. 3: a) Picture taken at 10 AM LT on Jan. 4 2005 at CARE site for warm fog case study. b) An example for ice fog case, the picture was taken at 9:30 AM LT on March 9 2006.

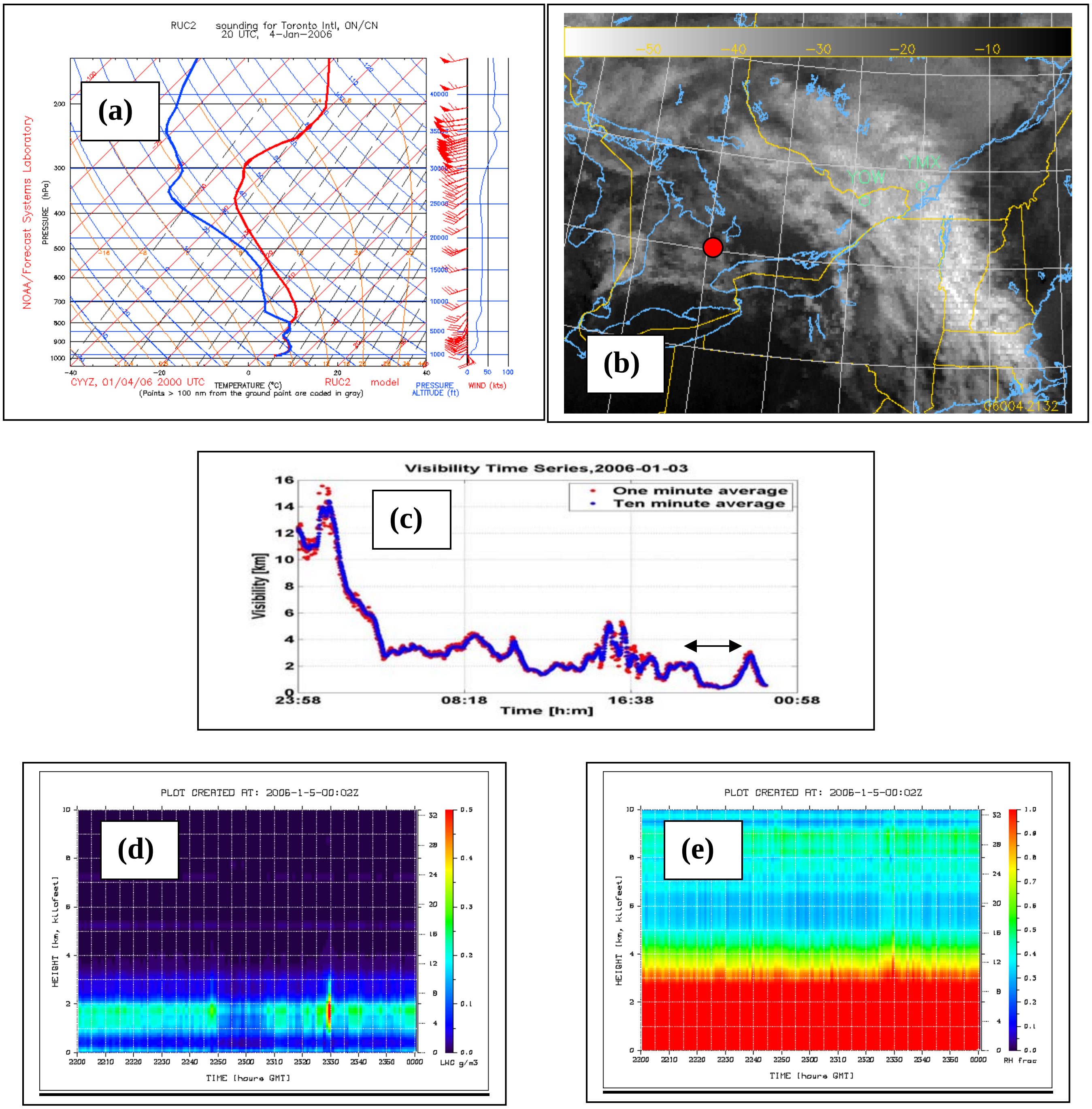

Fig. 4: a) RUC Model based radiosonde profile, b) The ch2 T from GOES at 2132 UTC, the filled red circle indicates project area, c) Vis time series at CARE, d) LWC time-height cross section from MWR3000, and e) The RHw time-height cross section from MWR3000. The exact time for fog is shown by a horizontal line with arrows in box c.

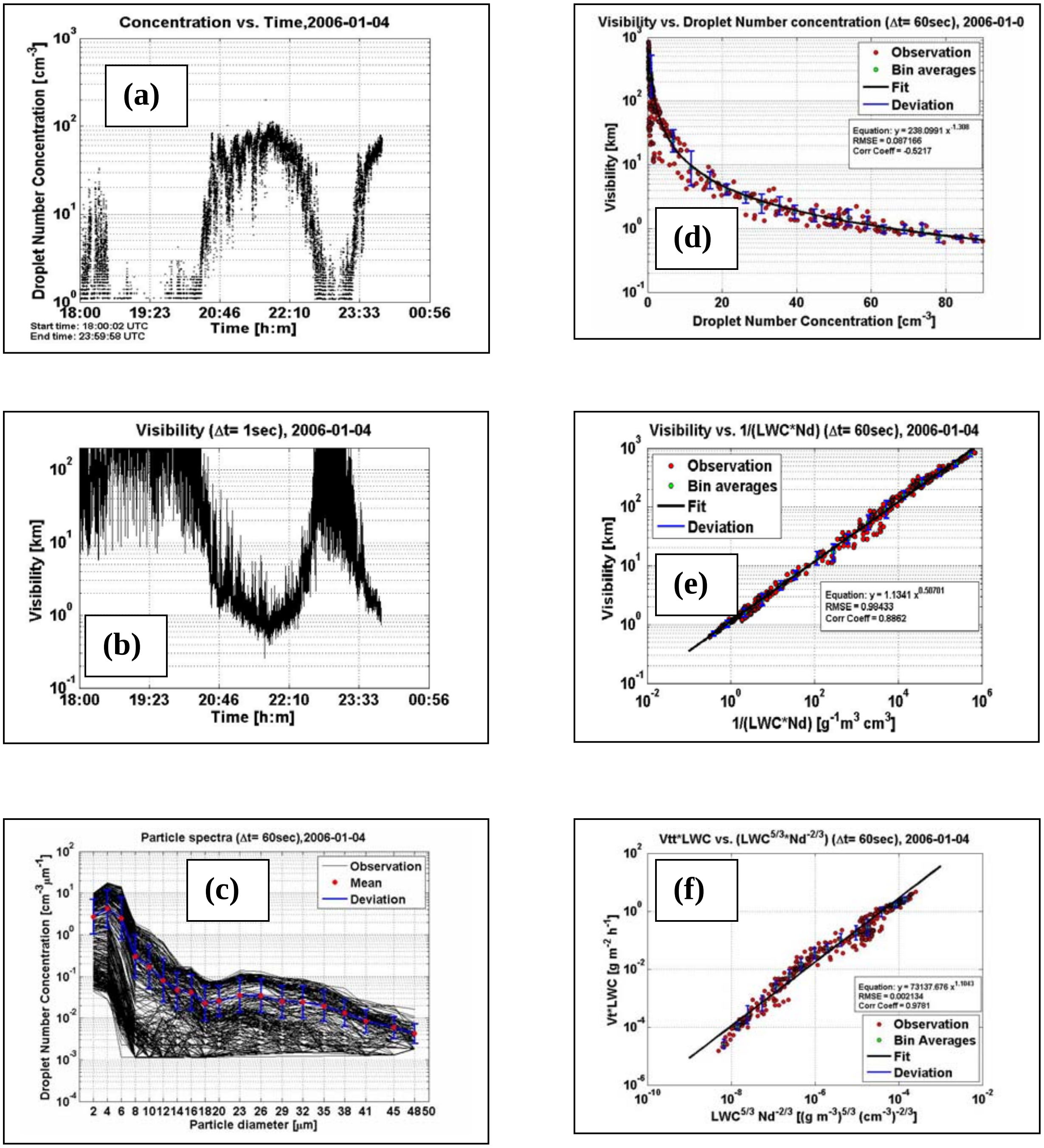

Fig. 5: Time series of droplet number concentration (a), and visibility (b) from FMD. The spectra for each second and values averaged over the bins together with standard deviations are shown in box c. The visibility versus N_d is shown in box d. Parameterizations of vis versus N_d and LWC is shown in box e. The parameterization of sampling rate of fog droplets is shown in box f. The data represents the Jan. 4 2006 case.

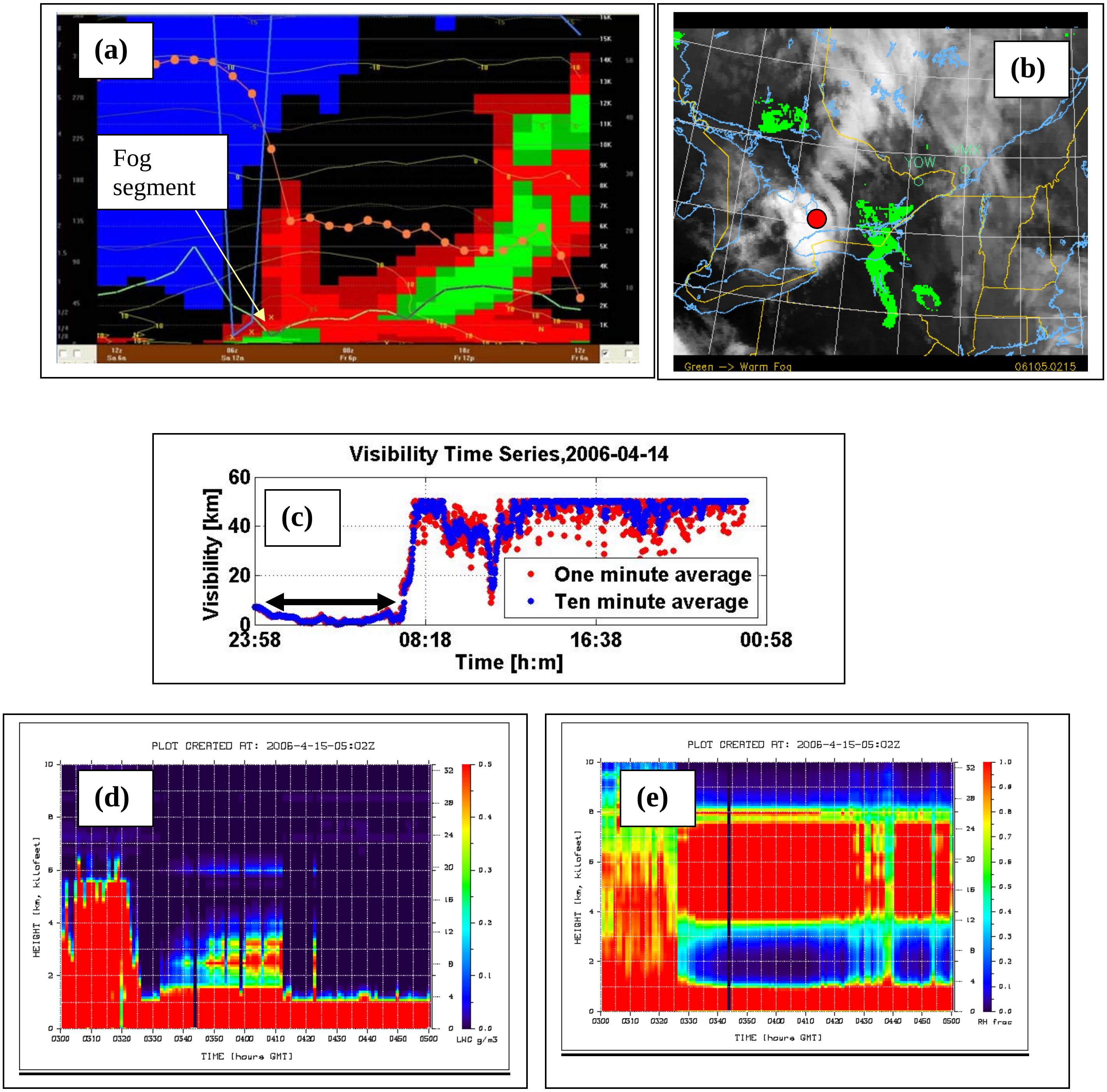

Fig. 6: a) Time-height cross section of model and observations based T, RHw, vis, and wind speed from BUFKIT, the green area shows RHw~100%, b) The GOES based fog region (green color) at 0215 UTC, the filled red circle indicates project area, c) Vis time series at CARE, d) LWC time-height cross section from MWR TP3000, and e) RHw time-height cross section from MWR TP3000. The exact time for fog is shown by a horizontal line with arrows in box c.

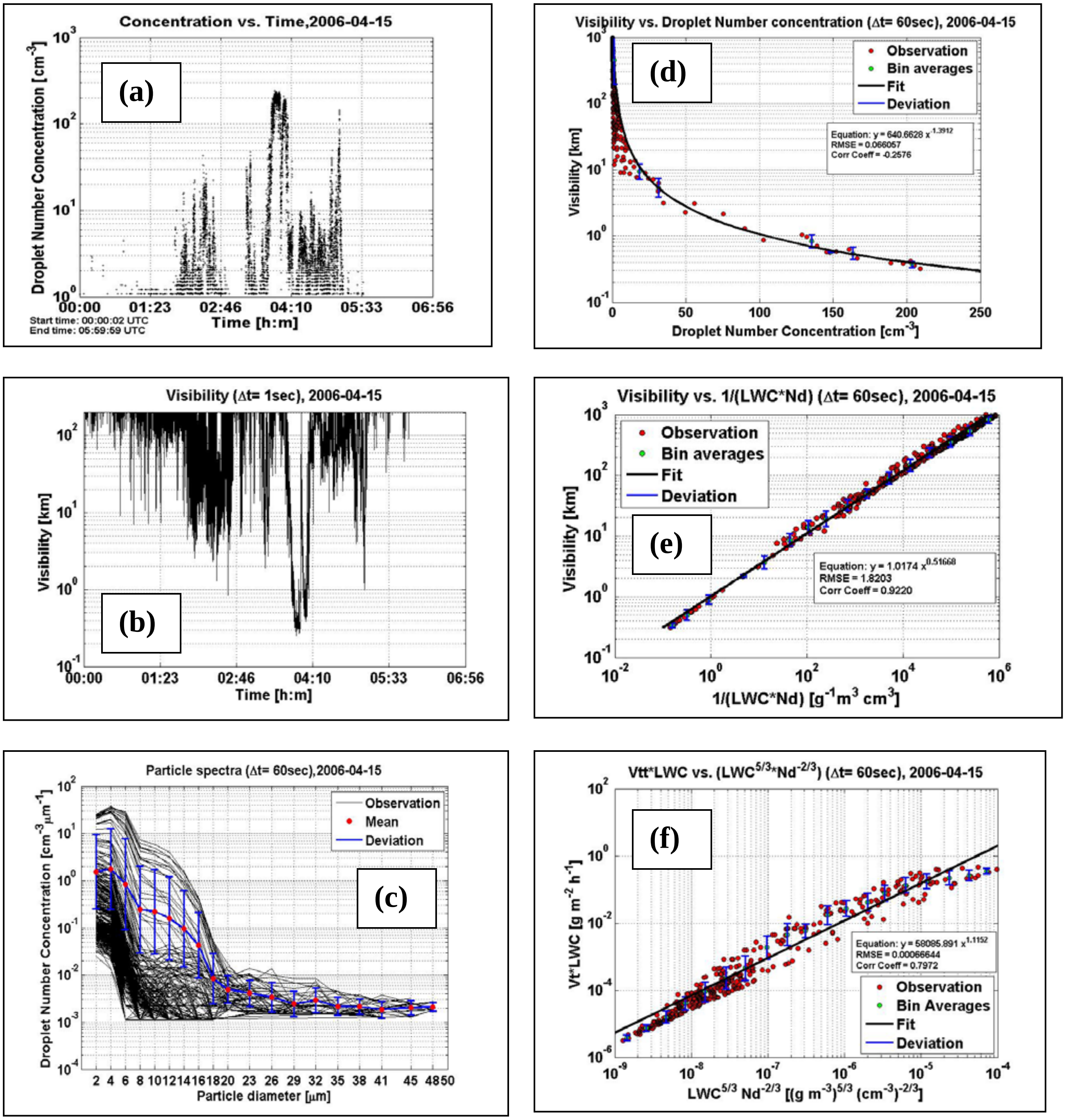

Fig. 7: Time series of droplet number concentration (a), and visibility (b) from FMD. The spectra for each second and values averaged over the bins together with standard deviations are shown in box c. The visibility versus N_d is shown in box d. Parameterizations of vis versus N_d and LWC is shown in box e. The parameterization of sampling rate of fog droplets is shown in box f. The data represents the April 15 2006 case.

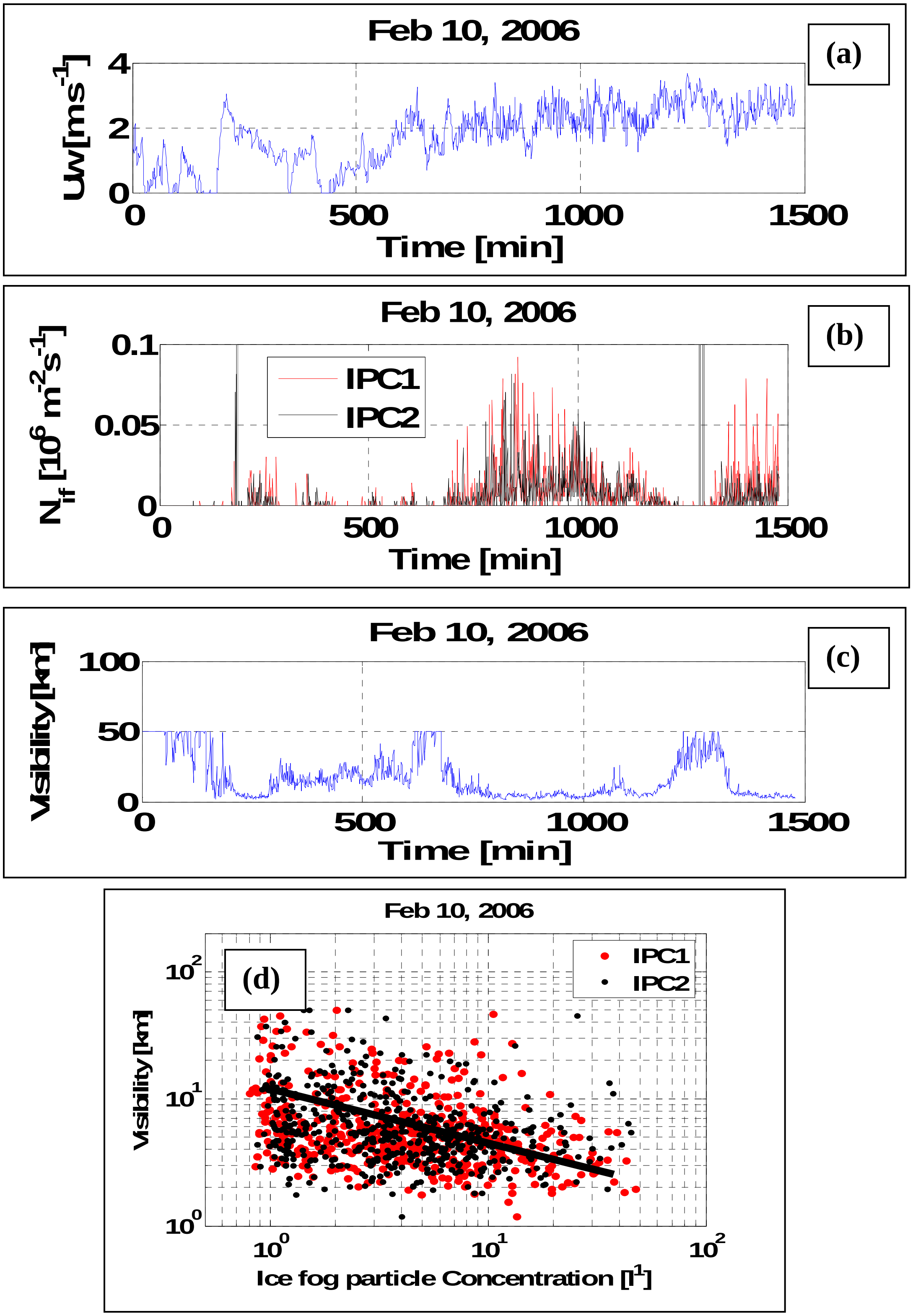

Fig. 8: Time series of horizontal wind (a), ice crystal mass flux (b), visibility (c), and visibility versus ice crystal number concentration (d). The black line is for the eye-fit to the data. The red and black color represents IPC1 at 0.7 m and IPC2 at 2.5 m. Both instruments were located at 10 m meteorological tower that included other conventional observations.